LAWRENCE
LIVERMORE
NATIONAL
LABORATORY

LLNL-TR-699228

Spent Fuel Ratio Estimates from Numerical Models in ALE3D

J. D. Margraf, T. A. Dunn

August 2, 2016

Disclaimer

This work performed under the auspices of the U.S. Department of Energy by Lawrence Livermore National Laboratory under Contract DE-AC52-07NA27344.

LLNL-XX-NNNNNN

Lawrence Livermore National Laboratory

Spent Fuel Ratio Estimates from Numerical Models in ALE3D

Jonathan D. Margraf and Timothy A. Dunn
Computational Engineering Division
Lawrence Livermore National Laboratory
7000 East Avenue
Livermore, California 94550

July 26, 2016

Disclaimer

Abstract

Potential threat of intentional sabotage of spent nuclear fuel storage facilities is of significant importance to national security. Paramount is the study of focused energy attacks on these materials and the potential release of aerosolized hazardous particulates into the environment. Depleted uranium oxide (DUO_2) is often chosen as a surrogate material for testing due to the unreasonable cost and safety demands for conducting full-scale tests with real spent nuclear fuel. To account for differences in mechanical response resulting in changes to particle distribution it is necessary to scale the DUO_2 results to get a proper measure for spent fuel. This is accomplished with the spent fuel ratio (SFR), the ratio of respirable aerosol mass released due to identical damage conditions between a spent fuel and a surrogate material like depleted uranium oxide (DUO_2). A very limited number of full-scale experiments have been carried out to capture this data, and the oft questioned validity of the results typically leads to overly-conservative risk estimates.

In the present work, the ALE3D hydrocode is used to simulate DUO_2 and spent nuclear fuel pellets impacted by metal jets. The results demonstrate an alternative approach to estimate the respirable release fraction of fragmented nuclear fuel.

Section 1

Introduction

1.1 Motivation

The goal of the current project is to understand the consequences of an attack on spent nuclear fuel (SNF) storage facilities. The main concern is a threat in which a high-energy device impacts the nuclear material, fractures the fuel rods, and leads to a release of hazardous material. The objective is to quantify the radioactive source that is dispersed into the environment.

Full-scale tests of security events are needed in order to measure the amount of released material. However, cost, safety, and environmental concerns complicate experiments with actual spent nuclear fuel. Therefore, it is desirable to use a less hazardous surrogate material in experiments. A common surrogate is depleted uranium dioxide (DUO_2). DUO_2 shares many material properties with actual spent nuclear fuel. However, SNF undergoes grain-scale material changes during its lifecycle. These changes include the creation of fission products, changes to the grain structure of the material, and the addition of voids into the material, which increases the porosity and changes the density. These changes are not expected to affect the bulk mechanical behavior of the material, but could have important fine-scale effects on the fracture and resulting particle size distribution of pulverized fragments. Therefore, measurements of the release fraction (the percentage of the material released into the environment) may be different using a surrogate compared to using actual SNF.

The ability to scale the release fraction measurements resulting from full-scale experiments using surrogate materials to the release fraction expected from actual SNF is critical to applying experimental data to regulatory decisions. The spent fuel ratio (SFR) provides this relationship. The SFR is defined as the ratio between the respirable aerosol mass of SNF released to the respirable mass released of a surrogate under otherwise identical conditions. Respirable aerosols are defined as particles with an aerodynamic equivalent diameter of less than 10 micrometers. Previous attempts to quantify the SFR have resulted in a large discrepancy in values, varying from 0.42 to 12 (Durbin, et al., 2015). The uncertainty in these estimates has resulted in overly conservative risk evaluations.

1.2 Code Description

In the present work, computational modeling is used to demonstrate an approach to estimate the respirable release fraction of fragmented nuclear fuel. The ALE3D hydrocode is used to simulate DUO_2 and spent

nuclear fuel (SNF) pellets impacted by metal jets. The results of these simulations can be used to estimate the respirable release fraction based on emperical relations derived from experimental data.

ALE3D uses arbitrary Lagrangian-Eulerian (ALE) techniques and multi-physics packages to solve a wide range of engineering problems (McCallen, 2009). The advection and remap capabilities make it a useful tool for dynamic events such as explosions and high velocity impact. A large library of material models exists to fully define the state, strength, and failure properties for a specific choice of the user.

1.3 Estimation of the Respirable Fraction

The resulting particle size distribution from an impulse delivered by a high-energy device is the primary goal of this work. However, the required mesh resolution to accurately capture such details at the micron scale is currently not feasible with current computational capabilities. This can be circumvented because previous studies have demonstrated that for brittle materials the fragment size distributions follow power law scaling. Durbin et al. (2015) has shown that the respirable release fraction of DUO_2 and SNF materials can be directly related to the energy density imparted to the material. Figure 1 plots the percentage of particles in the respirable range verses energy density for relevant experiments using DUO_2 and SNF. The experimental data was taken from Molecke (2008), Ruhmann (1985), and Alvarez (1982).

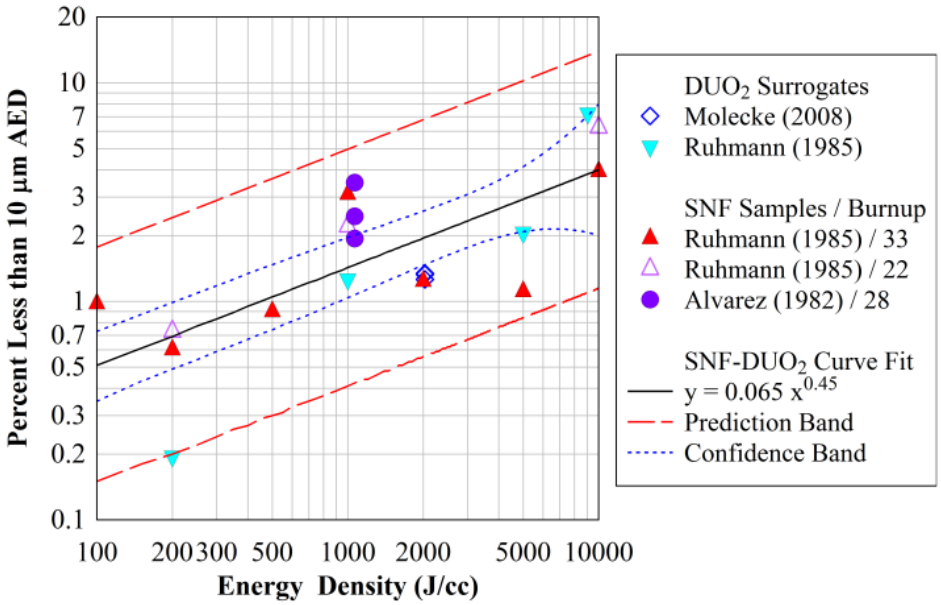

Figure 1: Mass Percent of Aerosol Generated as a Function of Energy Density (Durbin, 2015)

Therefore, since the respirable release fraction can be obtained from the energy density, the current approach is to use ALE3D to calculate the energy delivered to the fuel. The code reports a time history of the internal energy for the center pellet material. To compute the rise in the internal energy density the internal energy at a specific point in time is collected for all zones with the target material, the sum is obtained over all contributing zones, and divided by the initial volume of the center pellet. Thus the energy density at time t_i is calculated

$$ed_i = \frac{\sum_{zones} ie_i}{V_0}$$

When a converged energy density, ed_f, is obtained from the simulation the curve fit from Figure 1 can then be used to estimate the respirable release fraction, so

$$RRF = 0.065 * ed_f^{0.45}$$

Now equipped with a method to estimate the release rate, the spent fuel ratio can soon be calculated. To achieve this end a model needs to be set up that can approximate both the baseline depleted uranium oxide as well as a spent nuclear fuel.

Section 2

Baseline Surrogate DUO_2 Calculations

2.1 Problem Setup

The computational model simulates a high-energy metal jet impacting a stack of fuel pellets. In the initial baseline calculations, the surrogate material is used in place of the fuel. The ALE3D model is represented in Figure 2. The geometry and material setup were chosen to match the calculations in Durbin et al. (2015) as closely as possible. A stack of seven surrogate depleted uranium (DUO_2) canisters are modeled in 3D using quarter symmetry in ALE3D. Each canister is approximately 15.2 millimeters tall and is sheathed by a Zircalloy shell. There is no space between the pellets in the current model. The outside diameter of the DUO_2 and Zircalloy are roughly 9.3 and 10.7 millimeters, respectively. The jet is represented by a copper cylinder 20 millimeters in length with an outside diameter of 2 millimeters. The copper jet is traveling at a speed of 7.8 kilometers per second directed at the center of the middle canister. Sufficient air surrounds the fuel rods both to capture the debris cloud after impact and to minimize unwanted boundary effects. Symmetry is prescribed on the front and bottom planes. The top surface of the canister stack is fixed. All other boundaries have pressure continuous, non-reflecting, outflow conditions specified.

Figure 3 shows some calculated snapshots of the copper jet impacting the center fuel pellet. The jet compresses and expands the fuel material, causing it to fracture into particles. The calculations represent the materials as a continuum and do not predict actual particle size distribution of the fragments. Although the figure provides a discrete representation of the fuel in the later times, this is a plotting artifact and is not an accurate representation of the fragment sizes.

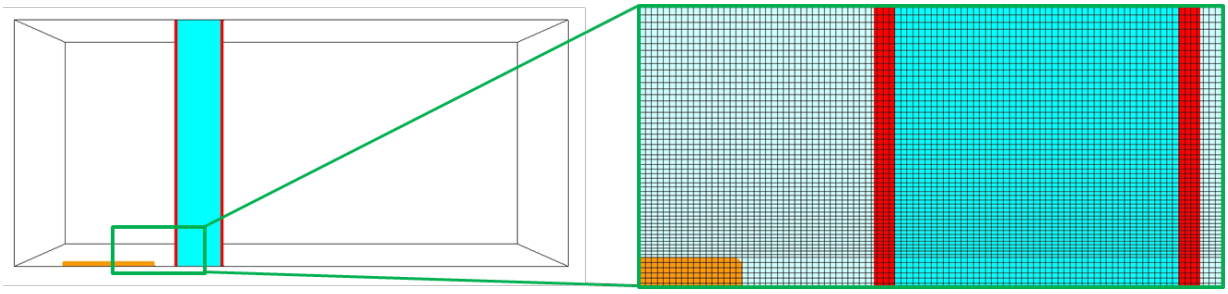

Figure 2: Finite element mesh of fuel rod and copper jet

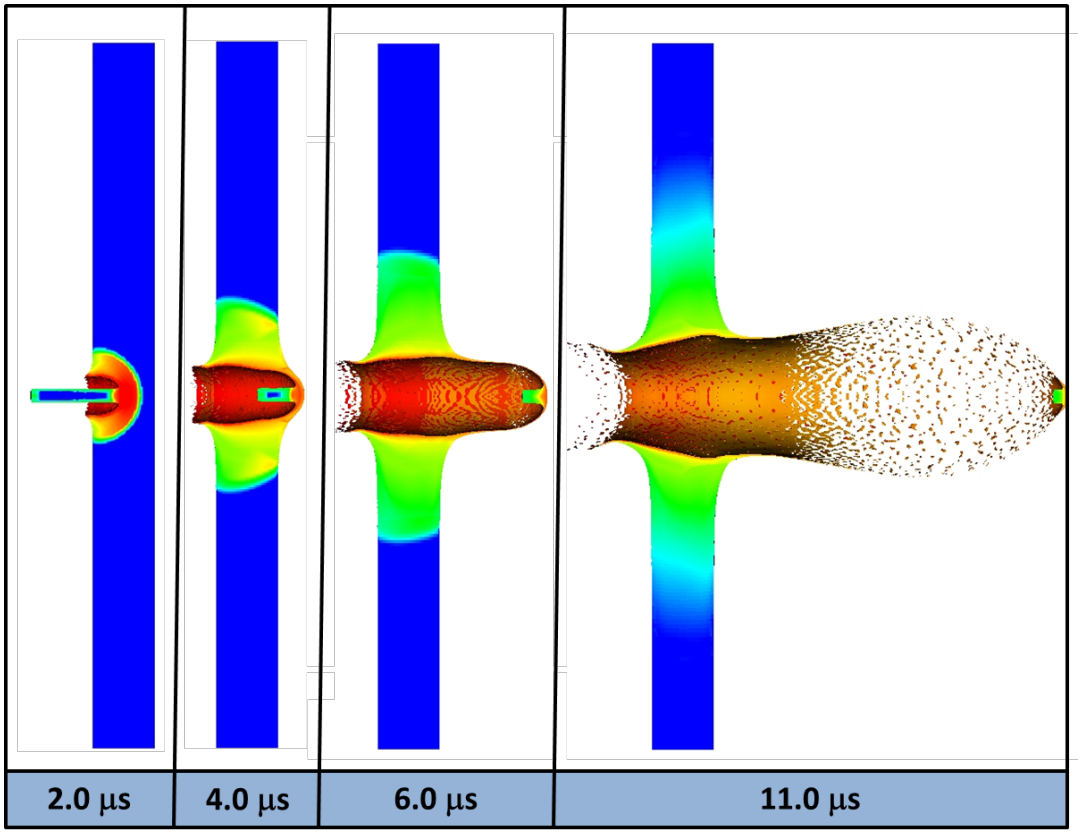

Figure 3: Penetration and resulting particle cloud. Color contours represent internal energy distribution in the fuel rod

2.2 Material Models

Both the depleted uranium oxide ($DU0_2$) and Zircalloy materials are represented with Johnson-Cook strength and failure models and a Mie-Gruneisen equation of state. The strength model has the form

$$Y = (A + B\varepsilon^n)\left(1 + C\ln\frac{\dot{\varepsilon}}{\dot{\varepsilon}_0}\right)(1 - T^{*m}) + C_4 p$$

$$T^* = \frac{T - T_{room}}{T_{melt} - T_{room}}$$

thereby capturing the dependence on strain, ε, strain rate, $\dot{\varepsilon}$, temperature, T, and pressure, p.
The Mie-Gruneisen equation of state is defined by

$$P = \begin{cases} \dfrac{\rho_0 c^2 \mu\left[1 + \left(1 - \frac{\gamma_0}{2}\right)\mu - \frac{a}{2}\mu^2\right]}{\left[1 - (S_1 - 1)\mu - S_2\frac{\mu^2}{\mu+1} - S_3\frac{\mu^3}{(\mu+1)^2}\right]^2} + (\gamma_0 + a\mu)E, & \mu > 0 \\ \rho_0 c^2 \mu + (\gamma_0 + a\mu)E\,, & \mu < 0 \end{cases}$$

giving the pressure as a function of compression, μ, and energy, E. Note that $\rho_0 c^2$ is the bulk modulus and compression is calculated by comparing the current density ρ to the initial density ρ_0.

$$\mu = \frac{\rho}{\rho_0} - 1$$

Johnson-Cook failure is governed by

$$\varepsilon_f = \left(D_1 + D_2 e^{D_3 \frac{p}{\bar{\sigma}}}\right)\left(1 + D_4 \ln \frac{\dot{\varepsilon}}{\dot{\varepsilon}_0}\right)(1 + D_5 T^*)$$

providing a dependence on triaxiality, $p/\bar{\sigma}$, strain rate, $\dot{\varepsilon}$, and the effective temperature, T^*. This failure model has the option of varying the parameters D_1 and D_2 from zone to zone, which can be crucial in providing realistic fracture patterns and behavior, though this is not used in the current scope of this study.

The necessary parameters for each material were chosen to match Durbin et al. (2015). These constants are reported in the appendix (Table 2).

2.3 Baseline Results and Mesh Convergence

The initial calculations were completed with 5 levels of mesh refinement. Figure 4 plots the energy density as a function of time for the simulations on each mesh. The figure shows good mesh convergence for the initial simulations, while the two highest refinements show nearly identical results. The finer mesh, with a total of 11.3 million zones, is utilized for all subsequent simulations.

Each curve in the figure exhibits the same behavior. As the jet hits the fuel the energy increases as the fuel compresses. Shortly after 2 microseconds, the energy hits its peak value and then starts to decrease as the fuel begins to expand. After about 4 microseconds, the energy hits another minimum. After this, the energy flattens out since the material is completely failed at this point and no further work is being done on the fuel material.

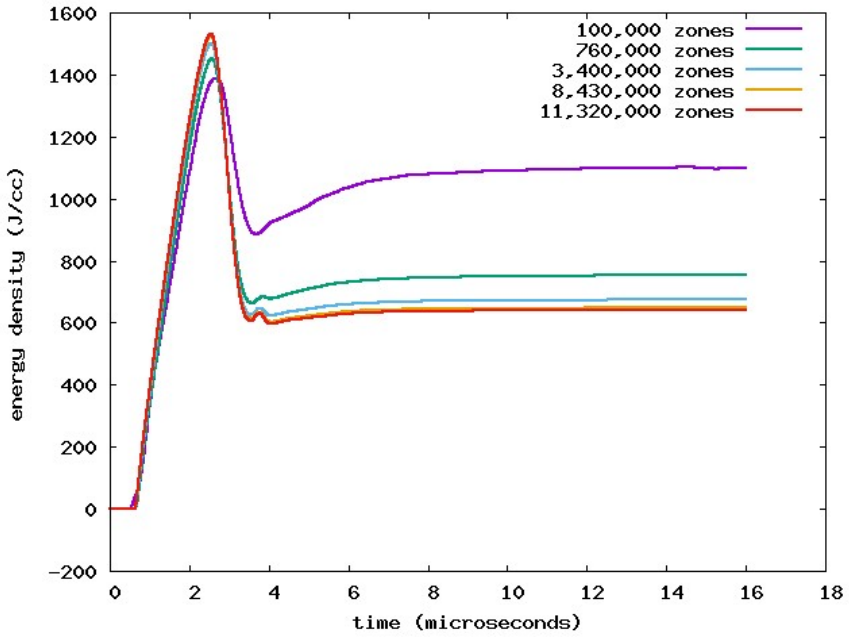

Figure 4: Energy density time history for surrogate DUO_2 indicating mesh convergence

Section 3

Spent Nuclear Fuel Calculations

Spent nuclear fuel undergoes material changes during its lifecycle. The primary change considered here is the change in density due to an increase in porosity. ALE3D accommodates porosity in a variety of ways. The details and potential consequences of 5 different approaches are explained in the following sections.

A total of four densities are simulated for each of the 5 different approaches. Each different density represents a porosity level corresponding to a particular level of fuel burnup. The geometric dimensions of the fuel rods are modified for each density in order to preserve the original mass of the fuel. The densities and dimensions are presented in Table 1.

3.1 Method 1: Reference Density Adjustment

The reference density is a property of the material model and is generally defined as the density of the material at a reference state corresponding to a zero pressure condition. The most straightforward way to modify the material density is to simply set the reference density to the desired material density, rather than the theoretical maximum packing density. While this ensures the proper mass, it does not account for material porosity. As the copper jet impacts the fuel, the material is compressed, followed by an expansion as the jet fully penetrates the fuel and the material is allowed to expand outwards (Figure 5).

Figure 6 shows the energy density of the center pellet as a function of time. The plot shows 4 different simulations corresponding to different initial densities of the fuel material. Similar to the baseline calculations, the current plot shows that as the jet hits the fuel, the energy increases then decreases as the fuel compresses and expands. The peak energy density at the end of the compression stage is very similar regardless of density, ranging from 1520 to 1610 J/cc. The residual energy density is also very similar from 645 to 670 J/cc. The likenesses might be best explained by comparing the relative volume of the material region in time. The compression phase is nearly identical which could explain the comparable peak energies. After the expansion phase, while more expansion may take place, the material is failed and can't sustain tension; therefore the energy density is for the most part unchanged from that point on. This method does not appear to accurately capture the effect of material porosity. This is expected since the material will have the same pressure response for each density.

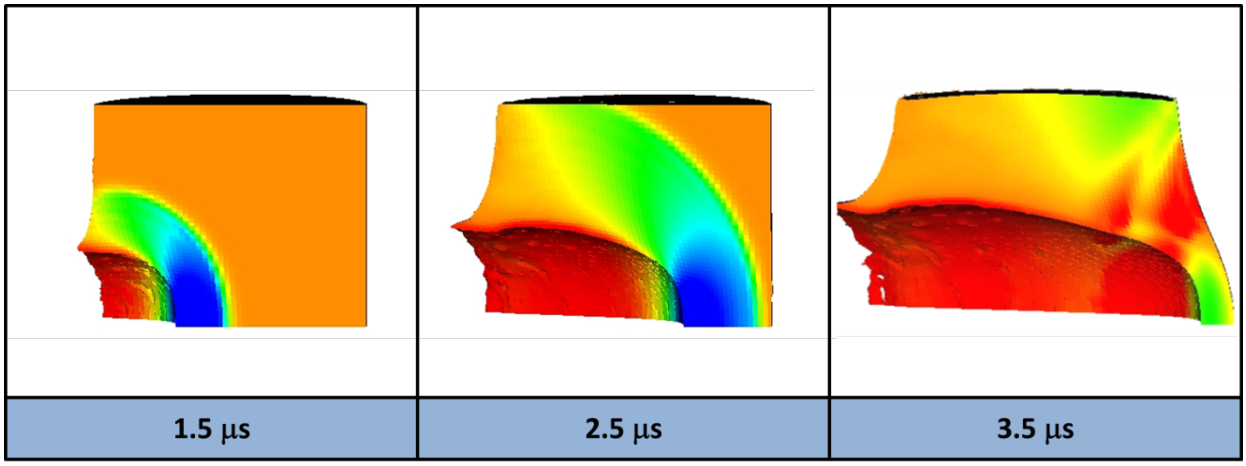

Figure 5: Method 1 relative volume plots. Material is compressed ahead of the copper jet, but expands at a later time. The blue color indicates the material is being compressed (high density), while the red color indicates the material is expanded (low density)

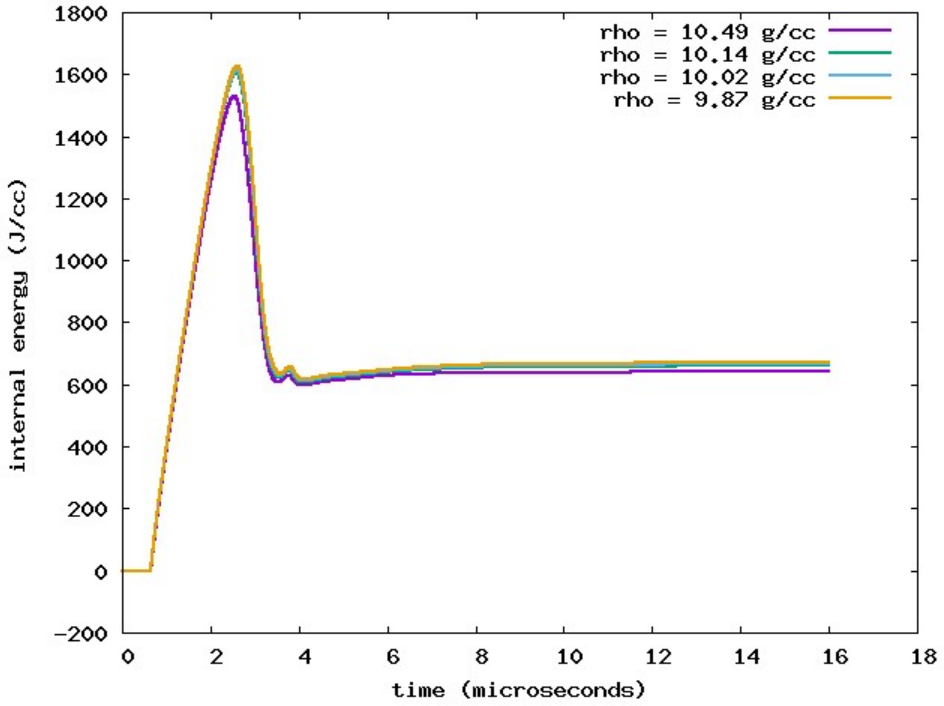

Figure 6: Internal energy density time history comparisons (Method 1)

3.2 Method 2: Initial Relative Volume Adjustment

The next approach used to vary the material density of the fuel is to modify the initial relative volume. The relative volume, v, is defined as the current volume of the material divided by the reference volume of the material. This is equivalent to

$$v = \frac{\rho_0}{\rho}$$

where ρ_0 is the reference density and ρ is the actual material density. By setting the reference density to the theoretical maximum packing density of the fuel (10.97 g/cc), the initial relative volume can be increased in order to obtain the reported initial density of the spent fuel. Since the material is initially in expansion, the pressure response is essentially zero. The pressure will become active after the material compresses. This is a crude way to approximate the collapse of voids within the fuel. However this may lead to spurious results, because the initial state of tension can cause premature failure due to the spall conditions being satisfied. In this problem, the jet impact causes the material to fail very quickly, and the effect of premature failure may be negligible. Figure 7 shows the relative volume in the fuel pellet. The behavior is similar to that seen in method 1, but the contour levels are different.

Figure 8 plots the energy density of the center pellet as a function of time for method 2. Differences in the 4 densities are immediately seen, as the peak and residual energy density increase with "porosity". This might also be best explained by the relative volume behavior. The higher initial relative volume models provide more available compression from the penetrator, and the difference from initial average relative volume and minimum average relative volume at ~2.5μs increases with porosity. This higher amount of compression could account for the larger peak energy densities, a trend that continues post failure to the reported residual values.

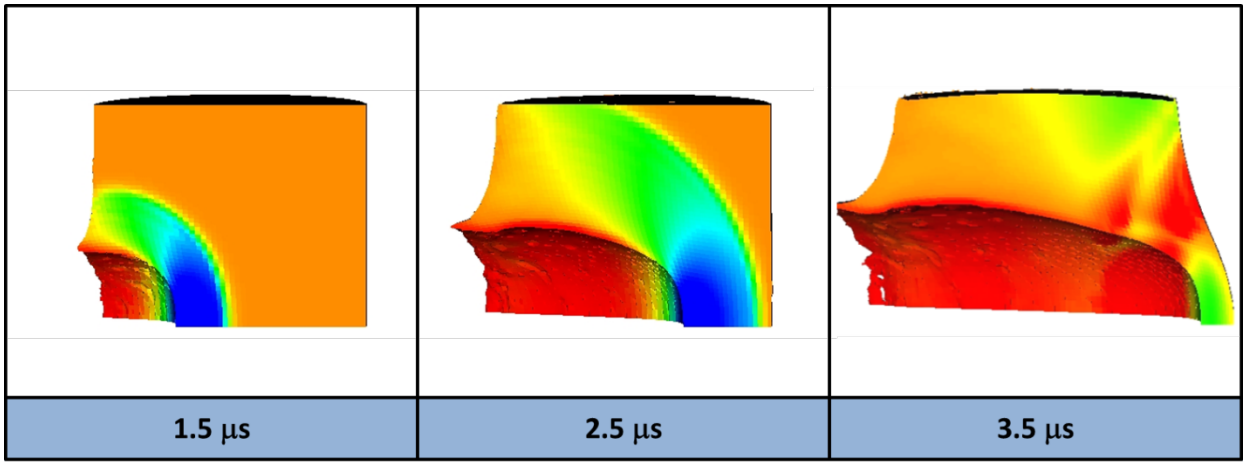

Figure 7: Method 2 relative volume plots. Material is compressed ahead of the copper jet (blue), but expands at a later time (red). The blue color indicates the material is being compressed (high density), while the red color indicates the material is expanded (low density)

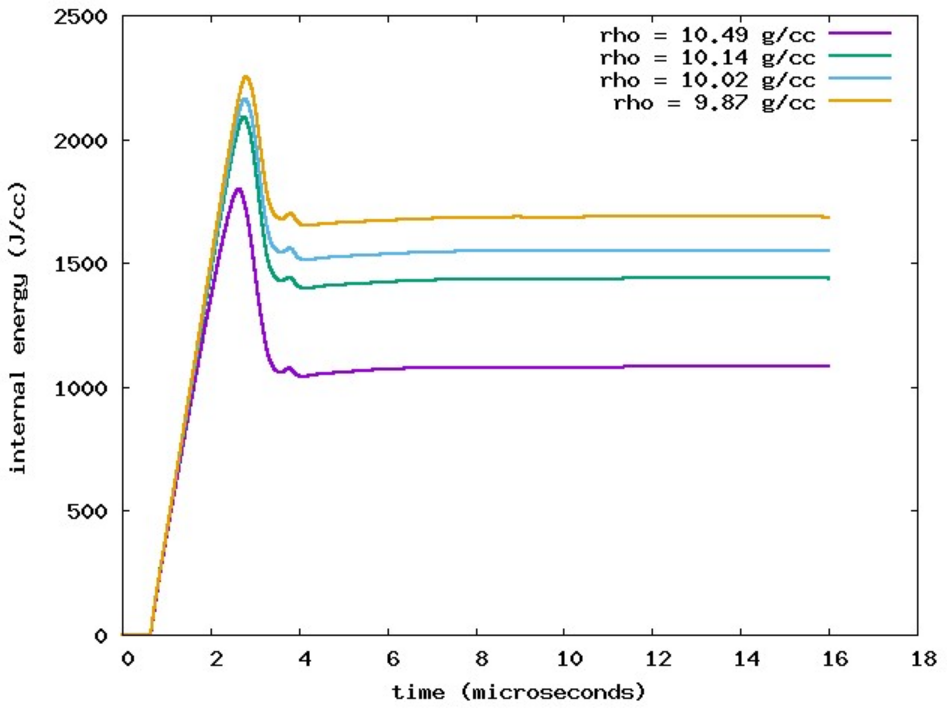

Figure 8: Internal energy density time history comparisons (Method 2)

3.3 Method 3: Void Material Insertion

In the third approach the porosity is accounted for by "shaping in" void throughout the material region. The SNF is given the theoretical reference density (10.97 g/cc), but by filling it with the proper distribution of voids, the actual density is reduced to the desired value. This option evenly distributes the void across the entire region, so each element initially has the same amount of void material. The void is quickly reduced as the penetrator makes its way through the fuel rod (Figure 9). Advection in mixed zones with small volume fractions can be problematic, which is seen as the newly advecting elements have a checkboard pattern of high void concentrations.

Figure 10 plots the energy density of the center pellet as a function of time for method 3. While the energy density does increase with porosity, it increases less with the void insertion approach than with method 2. Although the void insertion approach is an interesting concept that should be analyzed in greater detail, it does not appear to accurately represent the effect of porosity in the current calculations.

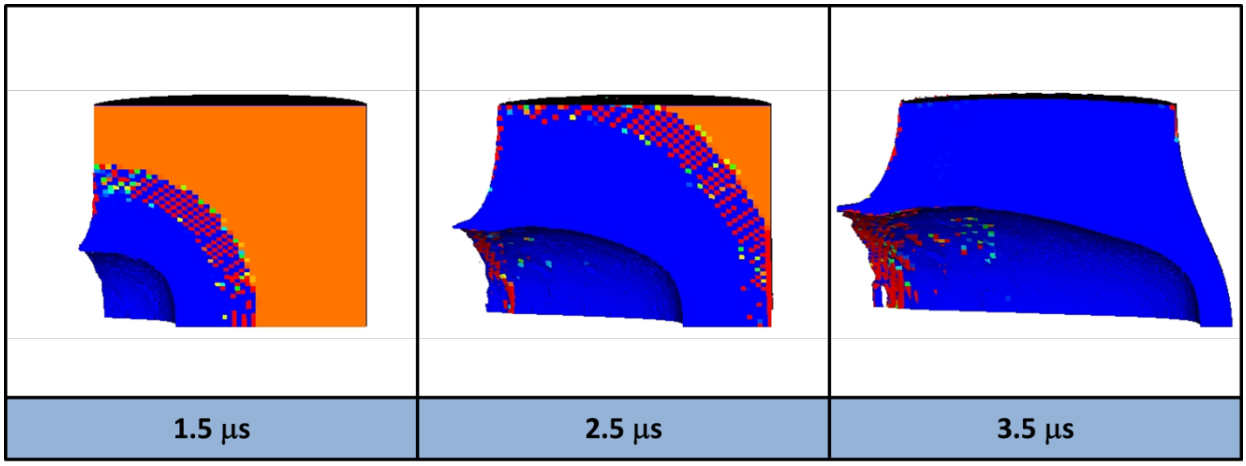

Figure 9: Method 3 volume fraction of voids. Voids are quickly removed as the material is compressed (blue)

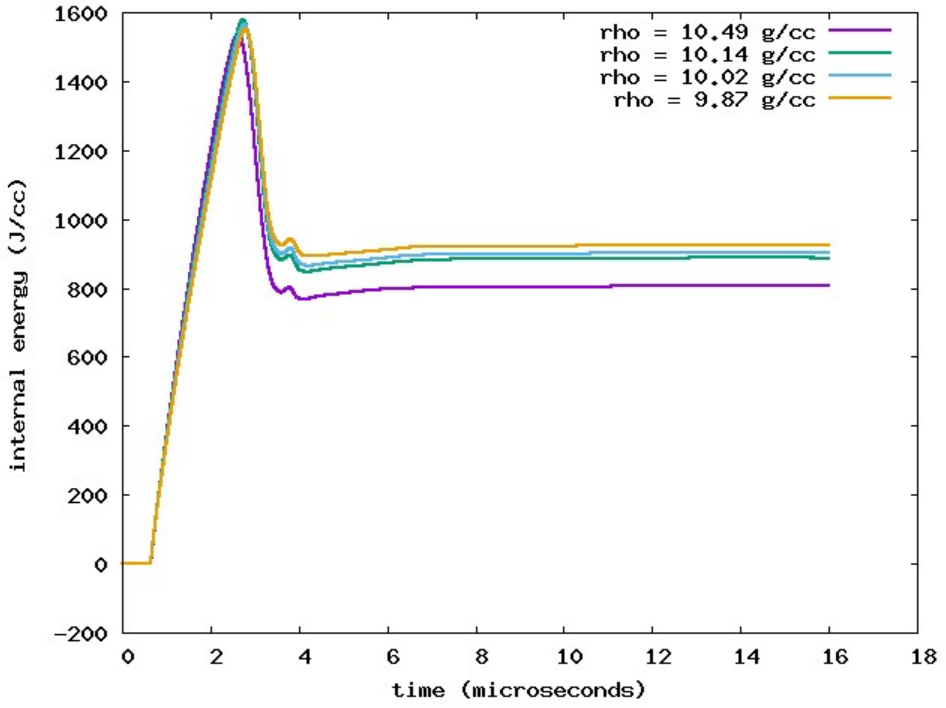

Figure 10: Internal energy density time history comparisons (Method 3)

3.4 Method 4: Gurson Material Model

Constitutive models have been developed to handle porosity, one of which is the Gurson model for ductile failure with damage. Porosity is tracked and plays an integral part in the strength of the material through the yield function. In the other methods the von Mises yield condition is determined through the effective stress, $\sigma_e = \sqrt{\frac{3}{2}\sigma'_{ij}\sigma'_{ij}}$. Yield occurs when $\sigma_e = Y$.

For the Gurson model the yield surface is replaced by

$$\sigma_e^2 - Y^2 - Y^2\left[2q_1 f^* \cosh\left(-\frac{3}{2}q_2\frac{P}{Y}\right) + {q_1}^2 {f^*}^2\right] = 0$$

The presence of voids is accounted for by the variable f^*. In the absence of voids $f^* = 0$ and the usual von Mises condition is recovered.

Voids are allowed to either compress or expand; behavior that can be seen in Figure 11. Changes to the strength and failure could play a significant factor in the behavior of this problem. By accounting for this, the Gurson model has a level of complexity that sets it apart from the other methods discussed thus far. The yield surface parameters (Table 3) were inherited from a similar, rigorously tested, material and the sensitivity to these values has not been explored. The Gurson model is the most advanced model in this study and possible tuning of each parameter to this specific material could be explored further in a future study. For more details on the Gurson model and its implementation in ALE3D, see Becker (2002) and Gurson (1977).

Figure 12 plots the energy density of the center pellet as a function of time for the Gurson model. Similar to method 2, the Gurson models predicts an increase in energy density with porosity. The energy values are slightly less than the results for method 2.

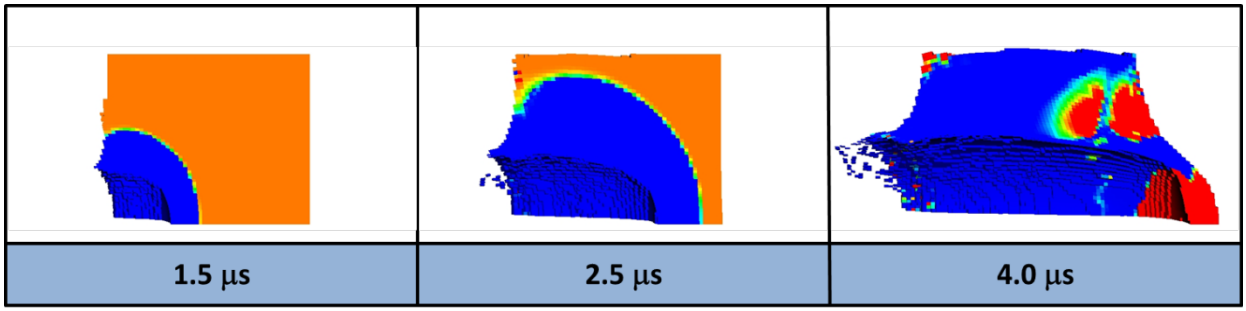

Figure 11: Method 4 volume fraction of voids. Voids are collapsed from compression (blue) and later expanded (red)

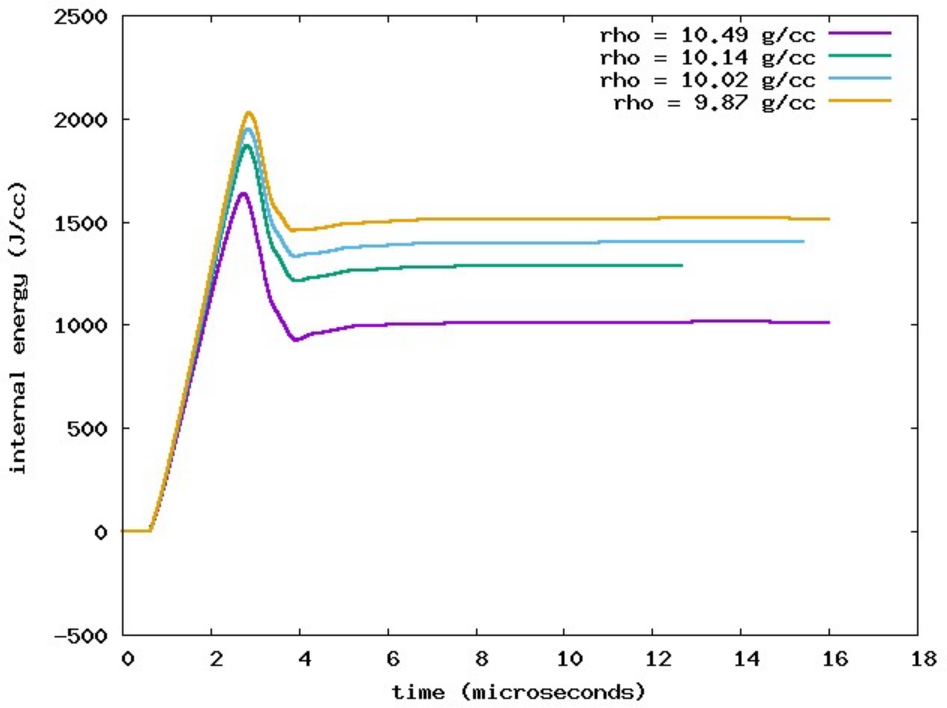

Figure 12: Internal energy density time history comparisons (Method 4)

3.5 Method 5: P-alpha Equation of State

The final approach used to model the porosity is the P-alpha model. The P-alpha model is new to ALE3D and was implemented as part of this project. In the P-alpha model, the material porosity is modeled through the equation of state. The pressure depends on the pressure of the solid (pore-free) material, calculated from the Mie-Gruneisen EOS, as well as a distention parameter which is directly related to the porosity. The distention parameter, alpha, has a predetermined elastic (reversible growing and expanding of pores) and plastic (irreversible crushing) behavior and is largely a function of the current pressure. Figure 13 demonstrates the linear elastic behavior by the four nearly horizontal lines on the left, and the plastic behavior that varies quadratically with pressure on the right. The parameters used to define these curves were matched to those used in Durbin et al. (2015). For more details on the P-alpha implementation see Wardlaw et al. (1996).

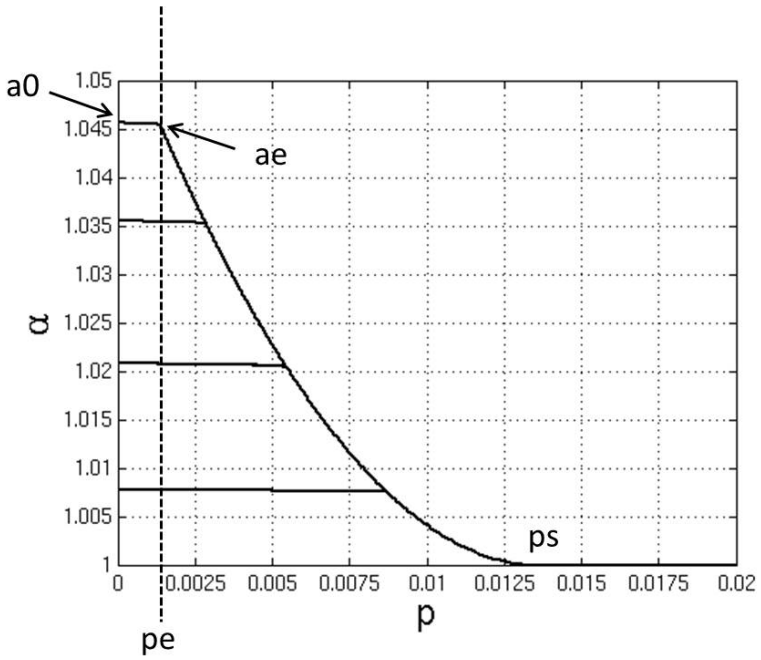

Figure 13: Distention parameter elastic/plastic behavior

Unlike the Gurson model, the porosity makes no changes to the strength or failure, but produces a pressure and relative volume response through the equation of state. It is also worth noting that once the pores are completely crushed they will not return. Figure 14 demonstrates that the pores are quickly crushed and remain that way, a fact that differentiates this approach from the Gurson model. This method may behave similar to the initial relative volume approach because an increase in initial relative volume is needed to account for the voids, however now without putting the material in an initial state of tension (Figure 15).

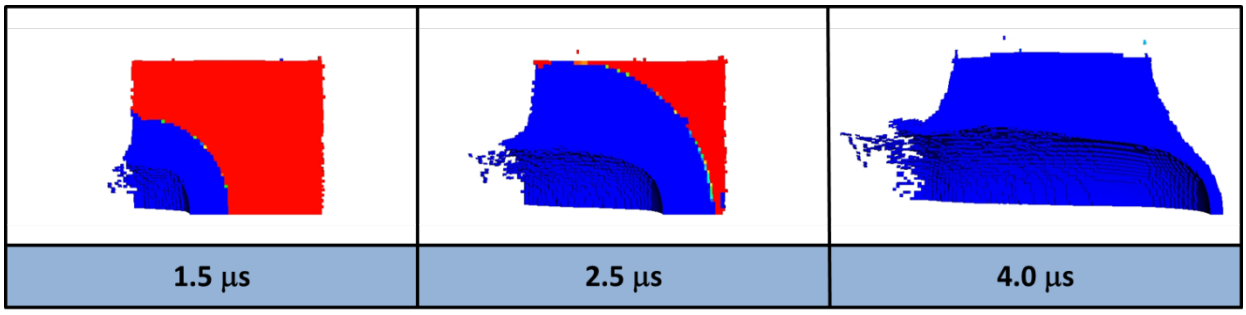

Figure 14: Method 5 volume fraction of voids. Voids are removed when material is compressed (blue) and do not return

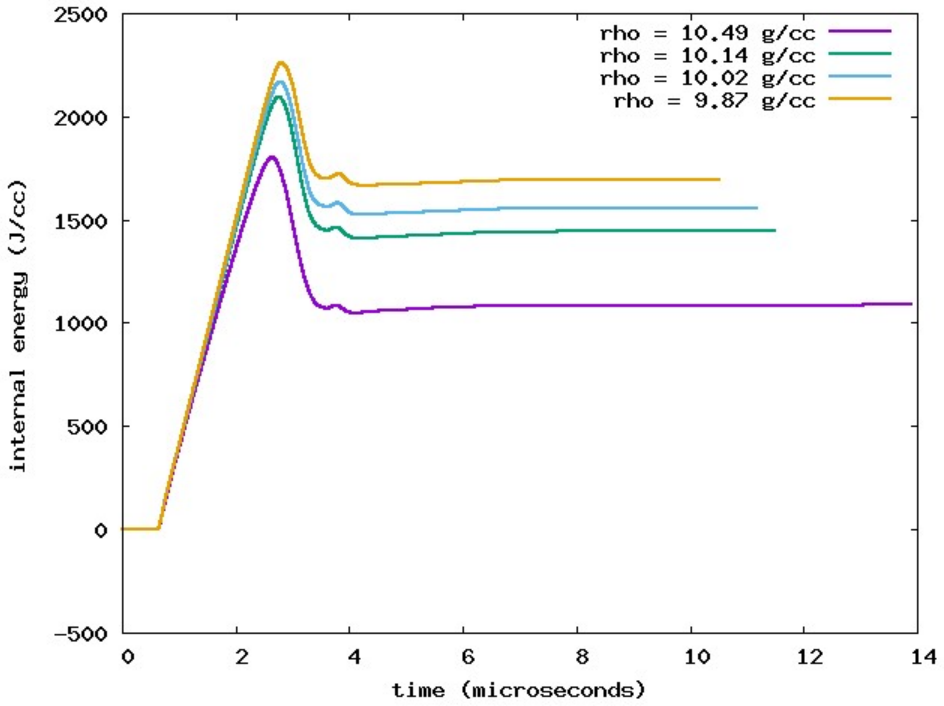

Figure 15: Internal energy density time history comparisons (Method 5)

Section 4

Comparison of the Spent Nuclear Fuel Porosity Models

Several attempts have been made to represent the porosity in ALE3D. Figures 16 and 17 compares the energy density results obtained by each approach. The most obvious conclusion is that a higher energy density is obtained as the porosity is increased. Increasing the reference density does not accurately represent porosity and therefore did not exhibit this behavior. Inserting void material does seem to have the expected behavior to a lesser degree, but the method needs to be scrutinized in greater detail. The Gurson model is widely used to model porous materials in ALE3D, and it gave meaningful results in this work even without modifying the yield parameters for this specific material. The initial relative volume should be used with caution due to premature spall, but it doesn't seem to make a large difference for this scenario. These results are remarkably similar to the P-alpha results, which do not have the described spall issue. The P-alpha model is a new implementation to ALE3D and looks to be a useful capability for modeling material porosity in ALE3D.

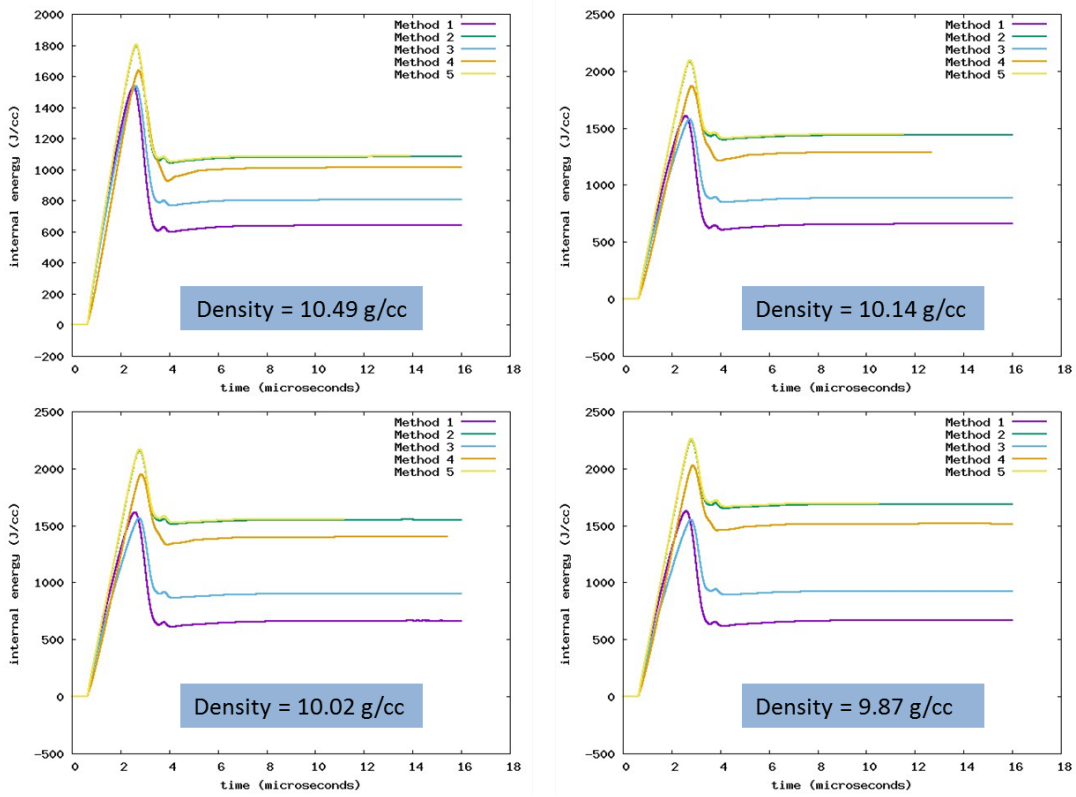

Figure 16: Internal energy density time history comparisons between methods

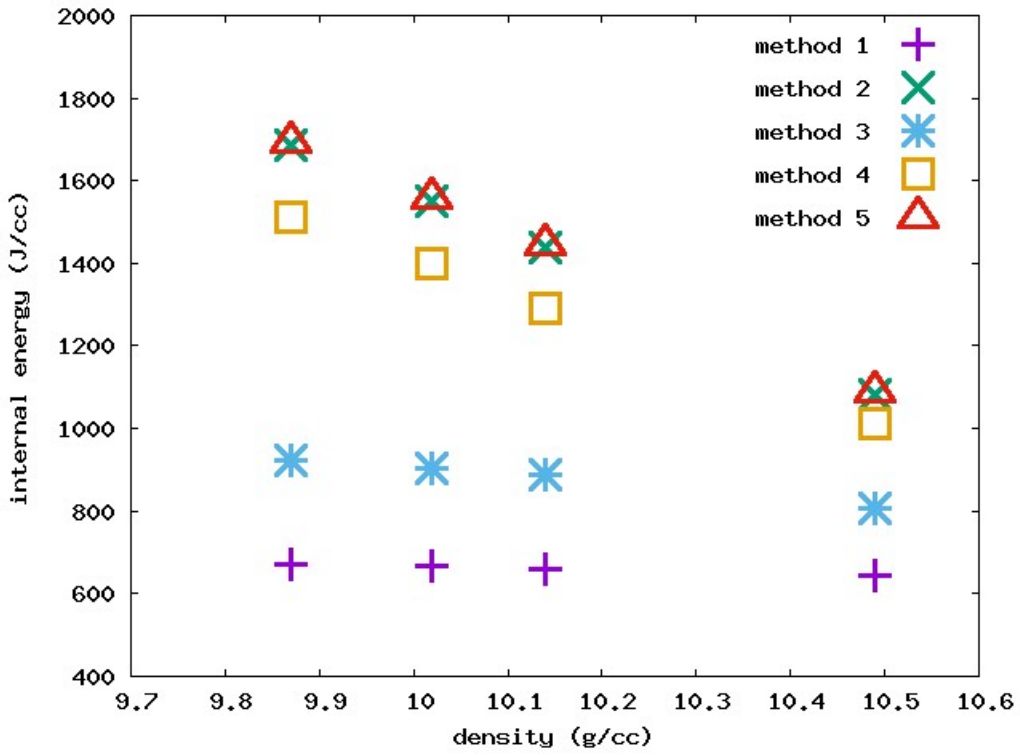

Figure 17: Method comparison on final internal energy density as a function of material density (initial porosity)

Section 5

The Release Fraction and Spent Fuel Ratio

With a process to estimate the resulting energy density of surrogate DUO_2 and spent nuclear fuels of various densities, along with a method to convert the energy density to a respirable release fraction (Durbin, et al., 2015), the spent fuel ratio can be readily obtained from these numerical models. The surrogate DUO_2 is represented by case 1 with a density of 10.49 g/cc and is assumed to have no burnup. The spent nuclear fuel is modeled with the densities of 10.14, 10.02, and 9.87 g/cc indicated burnup values of 45, 60, and 80 GWd/MTHM, respectively (Durbin, et al., 2015).

Respirable release fraction is estimated through Figure 1 and the energy densities reported from ALE3D and the calculated spent fuel ratio is obtained by dividing the release fraction of SNF to that of the surrogate DUO_2 (Figure 18).

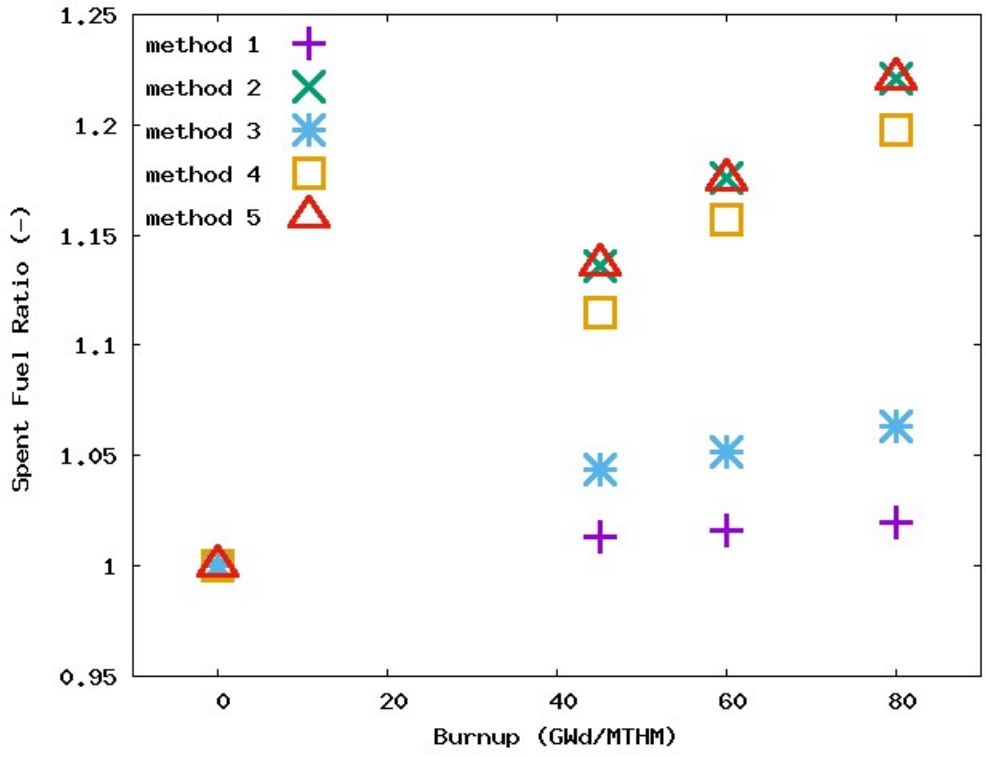

Figure 18: Method comparison on spent fuel ratio as a function of burnup

Section 6

Conclusions

Many high fidelity models were carried out in ALE3D to model the reaction of a high velocity copper jet into a DUO_2 fuel rod and to estimate the resulting energy density in the pellet. Similar results are obtained for spent nuclear fuel by decreasing the density and including porosity in a variety of methods. Converged solutions are available within several hours with these techniques, and show good capability to quickly determine numerical approximations to the spent fuel ratio.

Future work would be to explore other methods of measuring the SFR. The size of the particles likely depends on localized fracture behavior rather than a homogenized average value over a volume of material.

Various levels of spent nuclear fuel have been approximated by a simple change in density or porosity. Whether or not a broader set of mechanical properties need to be adjusted for a more accurate material representation is currently unknown.

Section 7

References

- Alverez, J.L., et al.,"Waste Forms Project: Correlation Testing", Idaho National Engineering Laboratory, Report EGG-PR-5590, (1982).
- Becker, R., "Ring fragmentation predictions using the Gurson model with material stability conditions as failure criteria", International Journal of Solids and Structures 39, (2002).
- Durbin, S.G., Lindgren, E.R., Wilke, J., and Jameson, K.J., "Numerical Estimation of the Spent Fuel Ratio", Sandia National Laboratories, Report SAND2015-2045 C, (2015).
- Gurson, A.L., "Continuum theory of ductile rupture by void nucleation and growth: part I-yield criteria and flow rules for porous ductile media". Journal of Engineering Materials and Technology 99, (1977).
- McCallen, R.C., "ALE3D: Arbitrary Lagrangian-Eulerian 2D and 3D Multiphysics Modeling and Simulation", Lawrence Livermore National Laboratory, Report LLNL-MI-413853, (2009).
- Molecke, M.A., et al., "Spent Fuel Sabotage Test Program, Characterization of aerosol Dispersal: Interim Final Report", Sandia National Laboratories, Report SAND2007-8070, (2008).
- Ruhmann, H., et al., "Research Program on the Behavior of Burnt-Up Fuel under Strong Mechanical Impacts", Kraftwerk Union, Report R 917/85/002, (1985).
- Wardlaw, B.W., Jr., McKeown, R., and Chen, H., "Implementation and Application of the P-α Equation of State in the Dysmas Code", Dahlgren Division Naval Surface Warfare Center, (1996).

Appendix A

Material Data and Material Model Parameters

Table 1: List of Material Data

Case	Reference Density (g/cc)	Density (g/cc)	DUO_2 OD (cm)	Zircalloy ID (cm)	Zircalloy OD (cm)	Canister Length (cm)
1	10.97	10.49	0.930	0.946	1.070	1.520
2	10.97	10.14	0.946	0.946	1.070	1.520
3	10.97	10.02	0.950	0.950	1.073	1.526
4	10.97	9.87	0.955	0.955	1.078	1.534

Table 2: Baseline Material Parameters

Parameter	Units	DUO_2	Zircalloy
T_0	K	298.0	298.0
cvav	Mbar cc / g / K	$1.102 * 10^{-5}$	$1.777 * 10^{-5}$
bulkMod	Mbar	1.054	0.707
Poisson's ratio	-	0.37	0.37
Johnson-Cook Hardening			
A	Mbar	$8.0 * 10^{-3}$	$4.45 * 10^{-3}$
B	Mbar	$4.5 * 10^{-3}$	$4.5 * 10^{-3}$
C	-	$1.6 * 10^{-2}$	$1.6 * 10^{-2}$
m	-	0.5	0.35
n	-	0.8	0.4
C4	-	0.0	0.0
T_{room}	K	293.0	293.0
T_{melt}	K	775.0	775.0
Mie-Gruneisen Equation of State			
S1	-	1.08	1.271
S2	-	0.0	0.0
S3	-	0.0	0.0
A	-	0.0	0.0
G0	-	1.0	1.09
Johnson-Cook Failure			
D1	-	0.08	0.4
D2	-	0.06	0.06
D3	-	-15.0	-15.0
D4	-	0.0	0.0
D5	-	0.0	0.0
Spall Pressure	Mbar	$-1.6 * 10^{-4}$	$-4.5 * 10^{-4}$

Table 3: Gurson Model Parameters

Parameter	Units	DUO_2	Zircalloy
q1	-	1.5	-
q2	-	1	-
f_c	-	0.2	-
f_f	-	0.4	-
ε_M	-	0.1	-
ε_S	-	0.03	-
σ_{hM}	Mbar	$1.0 * 10^{-3}$	-
σ_{hS}	Mbar	$2.5 * 10^{-4}$	-

Table 4: P-alpha Equation of State Parameters

Parameter	Units	DUO_2	Zircalloy
ce	cm / μs	0.3	-
pe	Mbar	$1.379 * 10^{-3}$	-
ps	Mbar	$1.379 * 10^{-2}$	-